AI-driven intelligent systems and robotics for advanced healthcare solutions – Original research article

INTERNATIONAL JOURNAL OF ADVANCED ROBOTIC SYSTEMS

International Journal of Advanced Robotic Systems
May–June 2026: 1–21

DOI: 10.1177/17298806261432729
journals.sagepub.com/home/arx
Sage

A standardised protocol for three-dimensional ankle kinematics: From motion capture to functional workspace analysis

Giovanni Mastrangelo[1], Betsy Dayana Marcela Chaparro Rico[2], Chelsea Starbuck[3], Matteo Russo[1], Marco Ceccarelli[1] and Daniele Cafolla[2]

Abstract

Understanding the complex biomechanics of the ankle is essential for advancing rehabilitation protocols and improving the design of assistive devices. This work proposes a standardised and reproducible protocol for the three-dimensional assessment of ankle kinematics using a marker-based gold-standard motion capture system. Ankle movements of 34 healthy adult women and men were investigated using a VICON motion capture system equipped with 12 infrared cameras. A total of 32 reflective markers were attached to the lower legs, feet and shoes of each participant to capture joint motion and foot–shoe interactions. Participants performed controlled plantarflexion–dorsiflexion, inversion–eversion and abduction–adduction movements, which were analysed using combined local coordinate frames to resolve ankle motion in all three anatomical planes. The ankle joint exhibited the greatest mobility in the frontal plane, with a maximum pitch angle of 106.5; dorsiflexion and plantarflexion were dominated by pitch motion, with an average range of 59.1° in pitch; inversion and eversion showed a more evenly distributed motion pattern, with average angular displacements of 37.4° in roll; abduction and adduction were characterised by yaw motion, with 28.3°. Results demonstrated consistent intra-subject repeatability across trials, with noticeable inter-subject variability, confirming the effectiveness of the proposed protocol in capturing natural variations in human motion. A secondary analysis revealed relative displacement between the foot and shoe, with an average slip of approximately 1 mm and peak values exceeding 10 mm in extreme cases, highlighting the importance of footwear-foot coupling in kinematic studies. The proposed methodology provides a robust foundation for the quantitative characterisation of ankle mobility, enabling reproducibility across laboratories and supporting future developments in rehabilitation robotics, ergonomic footwear design and motion analysis research.

Keywords

Experimental biomechanics, motion monitoring, motion capture system, ankle kinematics, functional workspace, rehabilitation, assistive devices

Received: 17 October 2025; accepted: 24 February 2026

Topic: I in Robotics; Human Robot/Machine Interaction
Topic Editor: Ankita Rajput
Associate Editor: Ankita Rajput

Introduction

The ankle plays a crucial biomechanical function in everyday movements including walking, running and jumping.[1] Among these, force transfer, stress absorption, maintaining balance, producing propulsion and adjusting to uneven terrain all depend on its healthy operation and all of these are intimately related to muscular health. Recent advancements in wearable sensing technologies, robotic assistance and

[1]Department of Industrial Engineering, LARM2: Laboratory of Robot Mechatronics, University of Rome "Tor Vergata", Rome, Italy
[2]Faculty of Science and Engineering, Intelligent Robotics Group, Department of Computer Science, Swansea University, Swansea, UK
[3]Faculty of Science and Engineering, Applied Sports, Technology, Exercise and Medicine Research Centre, Department of Sport and Exercise Sciences, Swansea University, Swansea, UK

Corresponding author:
Giovanni Mastrangelo, Department of Industrial Engineering, LARM2: Laboratory of Robot Mechatronics, University of Rome "Tor Vergata", 00133 Rome, Italy.
Email: giovanni.mastrangelo@alumni.uniroma2.eu

computational modelling have significantly expanded the ability to quantify and support ankle function during daily activities.[2,3] At the same time, the rapid development of ankle exoskeletons, rehabilitation robots and assistive devices has increased the demand for accurate biomechanical characterisation of ankle motion to ensure safe, effective and adaptive human–machine interaction.[4–7] Despite these technological advances, the ankle remains highly susceptible to injuries such as sprains, chronic instability and arthritis, which can significantly compromise mobility and quality of life.[8]

Understanding the biomechanics of the ankle has drawn more attention in recent years from both the clinical and technical domains. In the field of medicine, this information aids in the creation of successful rehabilitation plans,[9–12] and in engineering, it guides the creation of orthotics, prosthetics and assistive technology that restore or improve ankle function.[13–17] These systems rely heavily on precise descriptions of ankle joint kinematics, workspace boundaries and motion coupling to optimise control strategies, personalisation and adaptive assistance.[18–20] Despite significant progress in device design, sensing and control, a major challenge remains the lack of standardised and experimentally validated representations of the ankle's three-dimensional workspace, which are critical for both clinical assessment and engineering design. Within this context, the concept of the ankle workspace has emerged as a key biomechanical descriptor, providing a compact and quantitative representation of the joint's functional capabilities relevant to rehabilitation planning, performance evaluation and robotic system development..[21]

Additionally, the examination of ankle joint movement is essential in clinical and research contexts, providing significant insights into gait patterns, rehabilitation results and lower limb biomechanics.[22] Precise evaluation of ankle kinematics is crucial for comprehending pathological situations, directing therapeutic interventions, and enhancing athletic performance.[23]

Standardised procedures that are expressly designed for the analysis of ankle motion data are still lacking, despite the increasing availability of motion capture devices and computational tools.[24] Ankle mobility is inherently complex due to the interplay between multiple joints and planes of motion. As a result, accurate protocols that take into consideration anatomical diversity, marker placement precision, and suitable filtering and processing methods are necessary for the interpretation of motion capture data. The data acquisition parameters, joint modelling assumptions and analytical frameworks used in existing methodologies frequently vary, which causes discrepancies and restricts the comparability of results between investigations. The construction of specialised assistive devices, such as exoskeletons and wearable supports, that complement the joint's natural movements is made possible by an understanding of the ankle's workspace, which has important rehabilitation benefits. Furthermore, it helps patients with degenerative diseases experience less joint stress and increased energy efficiency. Through the identification of dangerous actions and the improvement of training methods, this type of analysis can help athletes perform at their best and avoid injuries. To address these inconsistencies, this work proposes a reproducible and standardised experimental procedure designed to ensure methodological comparability across laboratories.

Through the use of motion capture and analytical techniques, this work presents a novel methodology for describing ankle movement by analysing its workspace. A thorough depiction of the ankle's range of motion (ROM) as well as its geometric and kinetic behaviour during dynamic tasks may be made possible by this analytical procedure.

In parallel with advances in motion capture and biomechanical modelling, recent research has increasingly focused on position and displacement tracking control strategies for lower-limb rehabilitation and assistive devices. Accurate joint-level kinematic information is a fundamental prerequisite for these controllers, as it directly affects tracking precision, stability and user safety.[25]

Several studies have investigated ankle kinematics using motion capture systems, focusing on joint ROM, gait analysis or specific clinical conditions.[26] Classical works and subsequent experimental studies have provided valuable insights into ankle and subtalar joint behaviour, often relying on predefined joint coordinate systems and planar analyses.[27,28] More recent contributions have extended these approaches to rehabilitation robotics and assistive device design, where ankle kinematics are used to define reference trajectories or evaluate controller performance.[29,30] However, existing studies typically focus on either joint-level angular measurements or device-specific applications, without providing a fully standardised protocol that integrates three-dimensional workspace characterisation, consistent local reference frame definitions, and an explicit evaluation of foot–shoe coupling effects. The present work addresses this gap by proposing a unified experimental and analytical framework that enables reproducible three-dimensional ankle kinematic assessment and supports downstream applications in biomechanics, rehabilitation and control-oriented research.

The ankle joint is a complex anatomical mechanism that is necessary for movement and weight bearing. It serves as the point of connection between the leg and foot, facilitating essential movement and supporting the body during dynamic tasks. Mobility in the sagittal, frontal and transverse planes of the body is made possible by the ankle's articulating surfaces.[31]

Each plane experiences several forms of motion, as shown in Figure 1.[32]

Both dorsiflexion and plantarflexion, which take place around an axis via the medial and lateral malleoli, involve

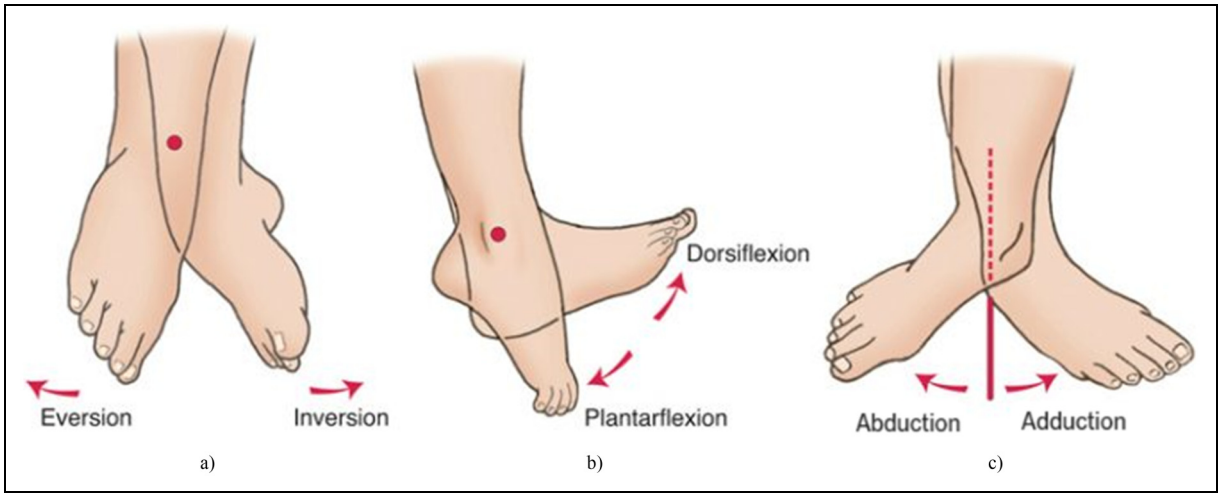

Figure 1. Ankle movements along the three axes of rotation: (a) eversion and inversion; (b) dorsiflexion and plantarflexion; (c) adduction and abduction.[32]

raising the foot toward the shin and pointing the foot downward, respectively, in the sagittal plane (Figure 1(b)). The rotational axis is located where the malleoli connect the longitudinal axis of the tibia, and inversion and eversion, respectively, characterise the inward and outward tilting of the foot in the frontal plane (Figure 1(a)). The transverse plane rotates around an axis that coincides with the long axis of the tibia, allowing the foot to move medially (adduction) or laterally (abduction) (Figure 1(c)).[33] These fundamental motions work together to create complex three-dimensional movements like pronation and supination.

For instance, pronation is a coordinated movement that turns the sole of the foot outward by combining dorsiflexion, eversion and abduction. These coordinated motions are essential for running, gait and surface adaptation.

The ankle experiences significant mechanical stresses: when walking, it frequently experiences force up to five times body weight, and when sprinting, it can experience forces up to 13 times. Assessment methods, age and cultural variables all affect its ROM. Sagittal plane ROM usually consists of 20° to 30° dorsiflexion and 38° to 46° plantarflexion. In general, frontal plane motion permits 10° to 17° of eversion and 14° to 22° of inversion. Adduction and abduction have different ranges in the transverse plane: 22° to 36° and 15° to 25°, respectively. Designing successful treatment therapies and mobility-enhancing devices requires a deep grasp of ankle biomechanics.

Activities that involve the abduction or adduction of the foot, like tracing alphabet letters, are still incorporated into rehabilitation protocols, even though some research indicates that the first two movements, plantarflexion and dorsiflexion, are crucial for proprioceptive training and ankle rehabilitation.[34]

Throughout the whole ROM, the thorough engagement of joints, tendons and muscles as a single unit is crucial in ankle rehabilitation. Furthermore, all of the trajectories necessary for rehabilitative activities can be performed using 3-DOF rotations.

The objective of this work is to establish and validate a standardised motion capture protocol capable of quantifying three-dimensional ankle kinematics and characterising its functional workspace.

The study is limited to kinematic workspace characterisation and does not address the dynamic stability or the neuromuscular control strategies of the ankle joint.

Materials and methods

This work was carried out part at the Intelligent Robotics Lab and part at Biomechanics Laboratory of Swansea University, with the participation of 34 healthy subjects: (20 males and 14 females) according to a protocol approved by the Ethics Committee of Swansea University with Research Ethics Approval Number that is 1 2024 11492 10405. The subjects voluntarily participated in this study. The inclusion criteria were the absence of diseases or injuries that can affect the ankle movements and age between 20 and 65 years. Inclusion or exclusion criteria were not imposed regarding height, weight or gender. Main characteristics of the 34 subjects included in the testing campaign are listed in Table 1.

Table 2 reports the maximum and minimum values for each parameter associated with the subjects who took part in the experimental campaign, highlighting the considerable heterogeneity of the sample. This variability reflects the deliberate inclusion of participants with diverse characteristics, aimed at ensuring a representative and comprehensive assessment of the investigated phenomena.

Figure 2 shows the experiment layout.

A VICON motion capture system,[35] which offers accurate tracking of the markers applied to the body, is used to record the movement. The sampling frequency of this

Table 1. Main characteristics of the volunteer subjects included in the study.

Subject	Age (years)	Weight (kg)	Height (m)	Gender	Shoe number (EU)
1	36	79	1.64	F	39
2	23	75	1.67	M	41
3	27	68	1.67	M	40
4	27	100	1.80	M	46
5	26	85	1.53	F	40
6	22	75	1.76	M	40
7	25	46	1.53	F	37
8	32	65	1.70	F	39
9	30	82	1.64	F	37
10	31	79	1.72	F	40
11	23	64	1.75	M	43
12	34	72	1.70	M	40
13	46	88	1.72	M	42
14	38	72	1.73	M	43
15	20	60	1.73	F	41
16	23	60	1.60	M	42
17	38	82	1.75	M	43
18	32	95	1.70	F	40
19	35	55	1.60	F	36
20	25	83	1.82	M	43
21	36	57	1.60	F	36
22	30	73	1.72	M	42
23	30	47	1.68	F	39
24	34	81	1.73	M	42
25	33	75	1.81	M	44
26	25	50	1.55	F	37
27	27	63	1.65	M	40
28	45	80	1.68	F	39
29	40	64	1.55	M	41
30	35	88	1.88	M	47
31	63	85	1.67	F	40
32	25	70	1.78	M	42
33	29	85	1.81	M	43
34	34	91	1.88	M	44

system is 250 Hz. To precisely record the three-dimensional locations of the markers, the VICON system uses 12 infrared cameras mounted on the walls of the laboratory in a square configuration, two cameras per side, plus one at each corner, so as to ensure full three-dimensional coverage of the movement area, and sophisticated software (Nexus, Figure 3[36]), guaranteeing high-quality data for analysing the ankle's ROM and movement patterns.

After each acquisition, all markers were manually labelled, as illustrated in Figure 3. Subsequently, the recorded trajectories were post-processed to identify any missing segments, which were then interpolated using the Nexus software tools. This procedure ensured continuity and accuracy in the reconstructed marker trajectories. Once the labelling and gap-filling steps were completed, the processed data were exported as .csv files for further post-processing and quantitative analysis. This step allowed for additional filtering, kinematic computation and the extraction of relevant parameters in external software environments.

Table 2. Summary of subjects' characteristics.

	Min	Max
Age (years)	20	63
Weight (kg)	46	100
Height (m)	1.53	1.88
Shoe number (EU)	36	47

A property configuration was developed for the implantation of markers on the ankle in accordance with the Davis et al. protocol,[37] a well-known technique for documenting human movement in biomechanical and kinematic research. Specifically created for 3D motion capture systems, this protocol developed a consistent mechanism for marker placement during motion data collecting. Its main goal is to ensure secure and accurate measurements by placing markers according to anatomical features, especially the epiphyses of bones. The motion capture system can track the object's 3D location and orientation in space by placing several markers on the rigid body. This allows for a thorough investigation of the dynamics of the object's movement.

Two markers were positioned at the femoral condyle positions, four markers were placed in a rectangular pattern on the shank, two markers were placed on the malleoli (one on the tibia and one on the fibula), one marker was placed on the heel, one on the first metatarsal, one on the second metatarsal, one on the fifth metatarsal and four markers were ultimately placed in a three-point star pattern on the calcaneus. This for both the right and left leg. While the three-point star pattern on the calcaneus was attached directly to the foot through a hole formed in the shoe, the markers on the heel, first, second and fifth metatarsals were placed directly on the shoe (as shown in the detailed view in Figure 4).

The complete marker configuration is shown in Figure 5.

This configuration made it possible to precisely track how the foot moved in relation to the shoe, guaranteeing reliable data collection while preserving the footwear's integrity throughout the testing processes.

The markers were systematically grouped following the schematic representation illustrated in Figure 6, which provides a clear overview of the adopted classification criteria and their underlying rationale.

This configuration allowed for a clear definition of the spatial relationships between the different segments and facilitated the accurate tracking of movement during the analysis. The grouping of markers into specific frames enhances the precision of kinematic measurements and ensures that each segment is tracked independently, allowing for detailed analysis of joint behaviour and segmental motion.

Figure 2. Experimental layout.

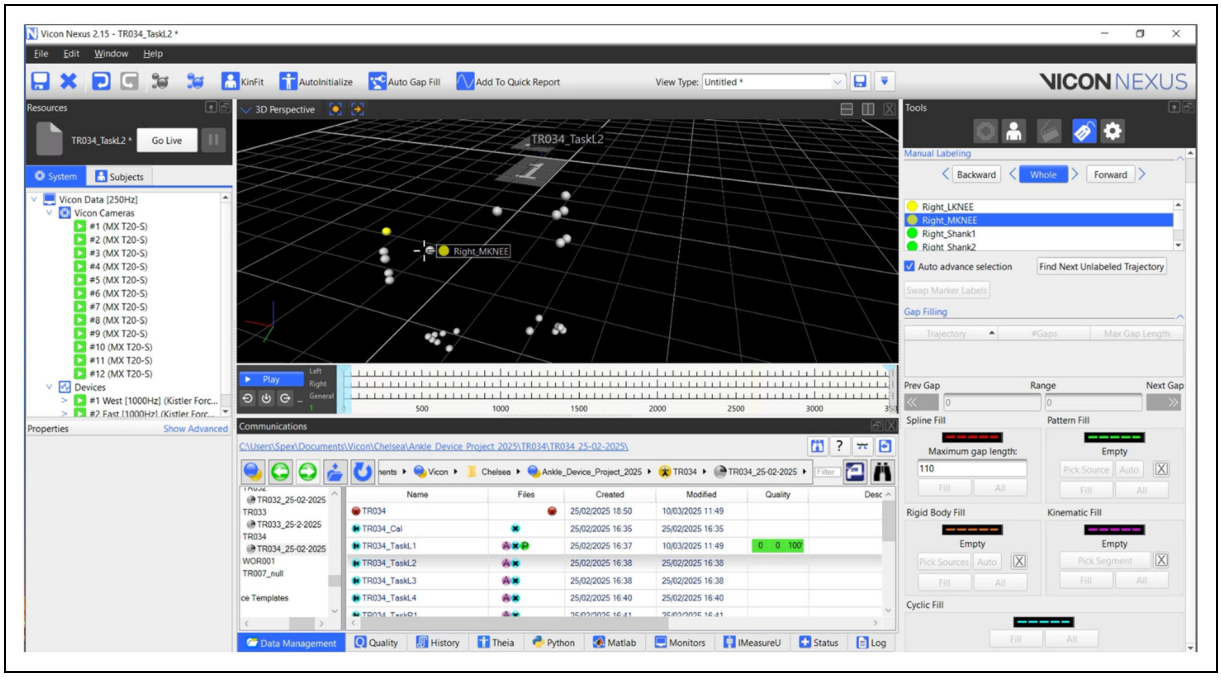

Figure 3. Nexus software interface.[36]

After the subject had been instrumented with the set of markers, they were seated on a stool positioned at the centre of the calibrated capture volume defined by 12 cameras. This setup allowed the leg to remain suspended, thereby enabling the execution of the desired foot movements without obstruction. The subject's leg was secured to the stool using a belt, in order to minimise any unwanted leg motion and to ensure that only the foot could move freely during the trials. Prior

Figure 4. Detail of the three-point calcaneal marker cluster inserted through a shoe aperture, ensuring direct skin contact for accurate tracking of foot motion relative to the shoe.

to the execution of each task, a short instructional video demonstrating the specific movement sequence was shown to each subject. This procedure was intended to facilitate the correct performance of the motion and to guarantee consistency and repeatability across all trials.

The protocol analysed is schematised as the following steps:

- Task 1: repetition of 3 complete movements as plantarflexion and dorsiflexion
- Task 2: repetition of 3 complete movements as inversion and eversion
- Task 3: repetition of 3 complete movements as adduction and abduction

These three tasks were performed for both the right and left foot. Figure 7 shows snapshot of the three different tasks for the left foot.

The UR model, shown in Figure 8,[38] represents the kinematic model proposed for the human ankle. In this model, the tibiotalar joint corresponds to the U-pair, while the subtalar joint corresponds to the R-pair. The size of the human talus is defined as the distance between the geometric centres of the U-pair and the R-pair.

To enable a comprehensive analysis of all ankle movements, a dedicated configuration of markers was proposed. This setting was intended to facilitate the interpretation of the experimental data and to ensure consistency across the different measurement conditions. The markers on the shank were grouped to form a rectangular frame, the markers on the shoe were grouped to define the shoe frame, the markers on the calcaneus were used to define the foot frame and the markers on the femoral condyles were connected to form a directional axis (dir1), as were the markers on the malleoli (dir2).

For every frame, a local reference system was established (shown in Figure 9), enabling further comparisons in both translational and rotational components: The four markers on the shank were used to create the S Frame, three of the four markers on the foot were used to define the F Frame, and three of the four markers on the shoe were used to create the M Frame.

All raw motion capture data were processed using MATLAB[39] software with a recursive Kalman filter to minimise measurement noise and ensure smooth reconstruction of three-dimensional positions. This approach ensured smooth and accurate angular profiles, preserving the dynamic characteristics of the movement. The filtered data were linearly interpolated in 1000 points and subsequently time-normalised on a scale from 0 to 100 for each trial (equation (1)). This normalisation procedure facilitated direct comparisons across subjects and movement types.

$$t_{norm} = \frac{t - t_{min}}{t_{max} - t_{min}} \cdot 100 \tag{1}$$

Angular displacements of the ankle joint were computed from the relative orientations of the local reference frames defined for the shank, foot and shoe. For each movement type: dorsiflexion/plantarflexion, inversion/eversion and adduction/abduction, the principal rotation component was identified according to the anatomical plane of motion. The secondary angular components were also analysed to assess coupling effects across axes.

For each frame (S, F and M), the corresponding markers were identified in order to construct the respective local reference systems. Once the three local coordinate systems had been established, the rotation matrix of each local frame with respect to the global reference system of the motion capture setup was computed (equations (2) and (3)).

$$R_i = \begin{bmatrix} u_x & v_x & w_x \\ u_y & v_y & w_y \\ u_z & v_z & w_z \end{bmatrix}, \; i = S, \; F, \; M \tag{2}$$

$$R_i = R_x \, R_y \, R_z, \; i = S, \; F, \; M \tag{3}$$

By decomposing the resulting rotation matrix R, the successive rotations around the x, y and z axes were obtained, following the chosen rotation sequence (equations (4)–(9)).[40]

$$R_x = \begin{bmatrix} 1 & 0 & 0 \\ 0 & cos\theta_x & -sin\theta_x \\ 0 & sin\theta_x & cos\theta_x \end{bmatrix} \tag{4}$$

$$R_y = \begin{bmatrix} cos\theta_y & 0 & sin\theta_y \\ 0 & 1 & 0 \\ -sin\theta_y & 0 & cos\theta_y \end{bmatrix} \tag{5}$$

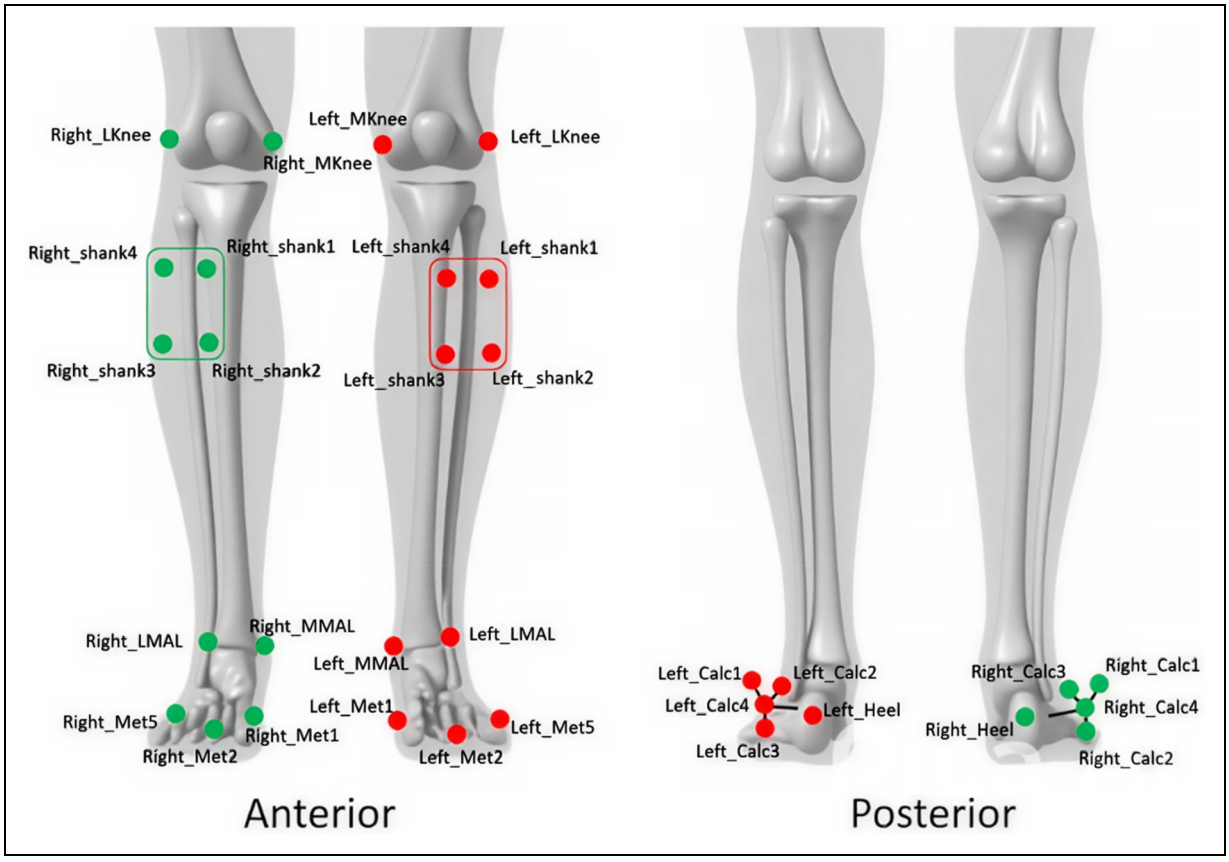

Figure 5. Markers setup of the shank and foot.

$$R_z = \begin{bmatrix} cos\theta_z & -sin\theta_z & 0 \\ sin\theta_z & cos\theta_z & 0 \\ 0 & 0 & 1 \end{bmatrix} \quad (6)$$

$$Pitch = arctg\left(\frac{R_{32}}{R_{33}}\right) \quad (7)$$

$$Roll = arctg\left(\frac{R_{21}}{R_{11}}\right) \quad (8)$$

$$Yaw = arctg\left(\frac{-R_{31}}{\sqrt{R_{32}^2 + R_{33}^2}}\right) \quad (9)$$

After determining the rotation angles of each local coordinate system, together with the corresponding origins, the relative rotations between the segments could be computed.

In particular, the ankle rotation angle was calculated as the relative rotation between the shank frame (Frame S) and the foot frame (Frame F). This approach allows for a precise quantification of the joint kinematics, providing a clear description of how the foot moves with respect to the shank within the global coordinate framework.

For each subject and trial, the ROM in terms of Pitch, Roll and Yaw, were computed as the differences between the corresponding angular components of the two reference frames. In other words, each rotational degree of freedom was expressed in terms of the relative orientation between

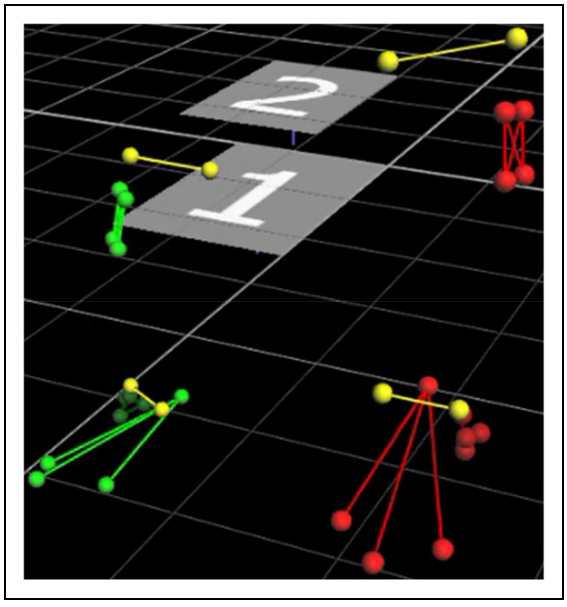

Figure 6. Schematic representation of the rigid bodies of the marker sets as visualised in Nexus software.

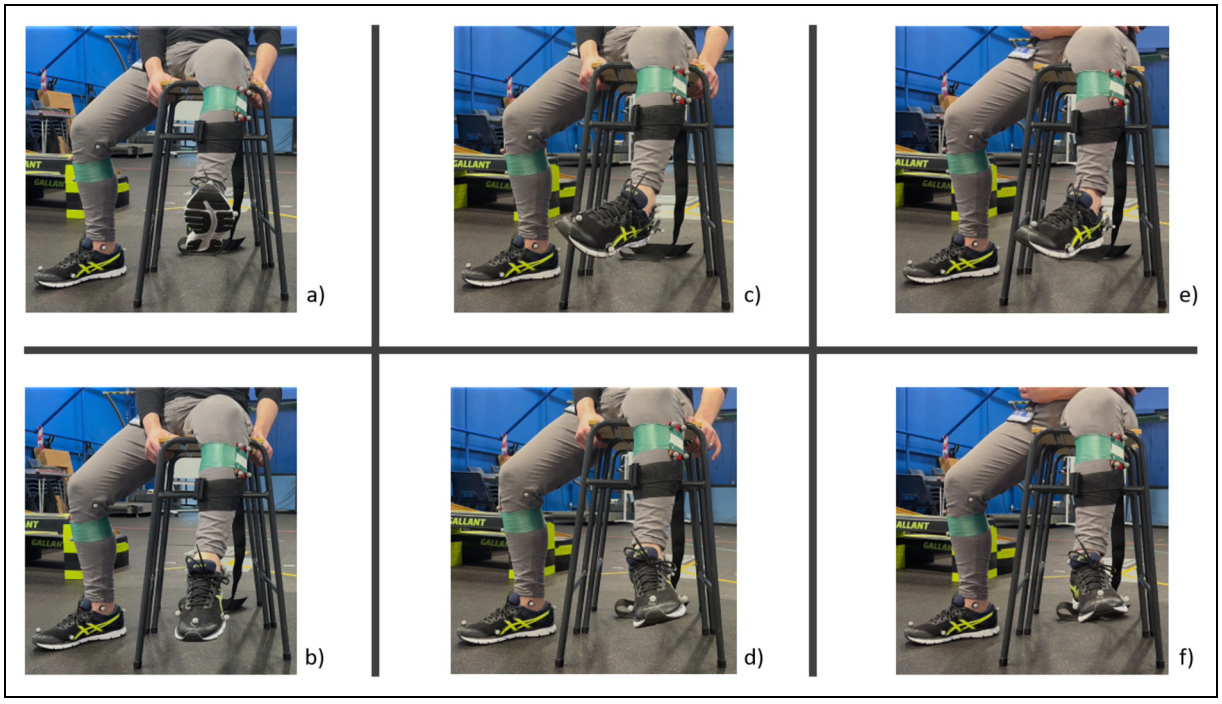

Figure 7. Snapshot of the three different tasks during the maximum range of motion for each movement of left foot: (a) dorsiflexion, (b) plantarflexion, (c) inversion, (d) eversion, (e) adduction, (f) abduction.

the two local coordinate systems. Once the angular values for each task had been computed, they were subsequently compared across trials in order to determine the mean and standard deviation.

The mean value of each angular variable was calculated according to the following expression (equation (10)):

$$\bar{x} = \frac{1}{1000} \sum_{i=1}^{1000} x_i, \ i = 1, \ \ldots, \ 1000 \tag{10}$$

Similarly, the standard deviation was computed as (equation (11)):

$$\sigma = \sqrt{\frac{1}{n-1} \sum_{i=1}^{n} (x_i - \bar{x})^2}, \ i = 1, \ \ldots, \ 1000 \tag{11}$$

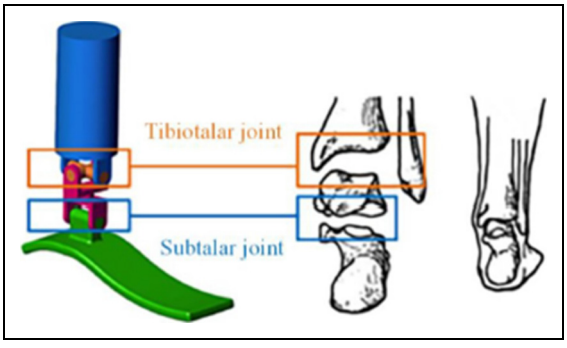

Figure 8. Schematic kinematic model of the ankle.[38]

These statistical measures were used to quantify the average behaviour of the angular displacement across trials and to evaluate the variability of the movement among repeated acquisitions. For each task, and for Pitch, Roll and Yaw, the following parameters were subsequently computed (equations (12)–(16)):

$$angle_{max} = \max(angle_i), \ i = 1, \ \ldots, \ 1000 \tag{12}$$

$$angle_{min} = \min(angle_i), \ i = 1, \ \ldots, \ 1000 \tag{13}$$

$$angle\ mean\ pick = \frac{1}{34} \sum_{k=1}^{34} \max(angle_i), \ i = 1, \ \ldots, \ 1000, \ k = 1, \ \ldots, \ 34 \tag{14}$$

$$angle\ mean\ valley = \frac{1}{34} \sum_{k=1}^{34} \min(angle_i), \ i = 1, \ \ldots, \ 1000, \ k = 1, \ \ldots, \ 34 \tag{15}$$

$$angle\ range\ mean = \frac{1}{34} \sum_{k=1}^{34} [\max(angle_i) - \min(angle_i)], \ i = 1, \ \ldots, \ 1000, \ k = 1, \ \ldots, \ 34 \tag{16}$$

Finally, the relative displacement between the foot (Frame F) and the shoe (Frame M) was computed as the absolute value of the translational differences between the

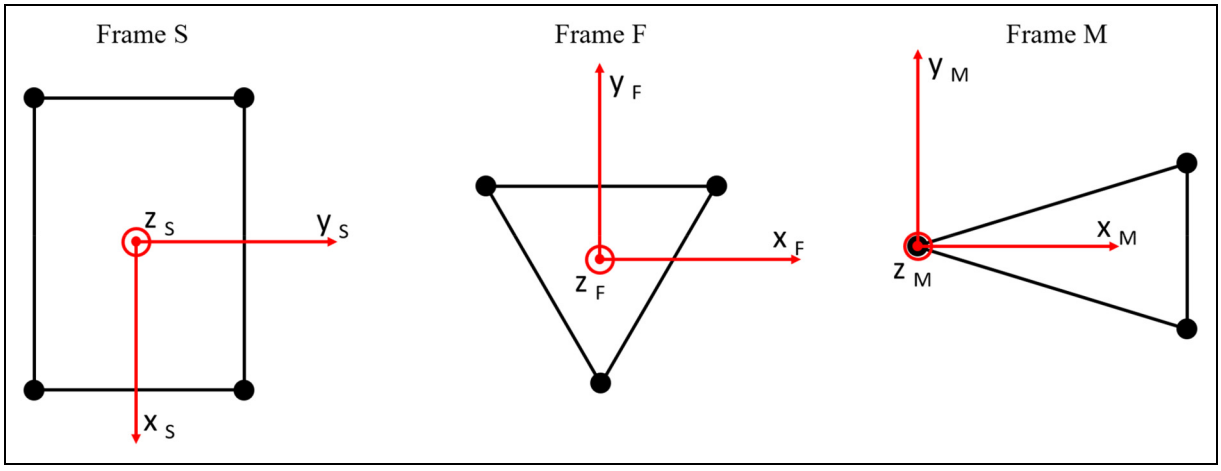

Figure 9. Local reference system for the S frame, F frame and M frame.

corresponding local frames for each point (equation (17)).

$$dist = \sqrt{(M_x - F_x)^2 + (M_y - F_y)^2 + (M_z - F_z)^2} \quad (17)$$

The mean, maximum and minimum values of this slip were extracted for each movement type and aggregated across subjects to evaluate the overall consistency and magnitude of the foot–shoe interaction.

Figure 10 shows the flowchart of the proposed procedure for data collection. In Section 1, subject setup, the system calibration is performed, followed by the reading and signing of the informed consent form, and the placement of the reflective markers on the anatomical landmarks. In Section 2, task performance, for each of the different tasks, a reference video demonstrating the desired performance is first shown to the participant. The subject then performs the task, and the acquired data are immediately checked for plausibility. If the recording is deemed unreliable, the task is repeated; otherwise, the data are saved for further processing. In Section 3, post processing, the markers are labelled and in cases of incomplete trajectories, a filling or reconstruction procedure is applied to ensure signal continuity, and the processed data are then exported in .csv format. Subsequently the data are filtered using a Kalman filter, interpolated to 1000 points to enable inter-trial comparison, and normalised to a [0–100] scale to ensure uniformity across traces. Finally, a statistical analysis is performed on the normalised datasets.

Results

The data obtained from the recordings were segmented according to the specific movement performed and subsequently analysed individually. Ankle movements are inherently complex, as they involve combined rotations occurring simultaneously across multiple axes. Although each motion is primarily oriented along one of the principal anatomical axes, secondary rotations around the remaining axes are also observed, as clearly illustrated in the corresponding plots.

Since each movement is examined independently, the analysis focuses on the principal component associated with the primary motion, in order to quantify the effective ROM for each case.

The first movement analysed corresponds to dorsiflexion and plantarflexion (Figure 11). For each test performed, the traces of the pitch, roll and yaw angles are presented separately, together with the corresponding mean values computed across trials.

Finally, a summary diagram is provided, reporting the mean values of all three angular components (±one standard deviation), along with the respective individual traces obtained from the 34 participants.

This representation enables a comprehensive visualisation of inter-subject variability and highlights the consistency of the observed kinematic patterns across the sample.

The sign of the measured angles was defined according to the direction of motion and the adopted reference frame. Positive pitch values correspond to dorsiflexion and negative values to plantarflexion. For the secondary motions, positive roll values were mainly associated with plantarflexion and negative values with dorsiflexion, whereas positive yaw values corresponded primarily to dorsiflexion and negative values to plantarflexion. For the pitch angle, the maximum value observed is 54.6°, whereas the minimum reached −51.9°. The peak points, corresponding to the dorsiflexion phase, exhibited a mean value of 26.7°, while the valley points, related to the plantarflexion phase, presented a mean value of −32.4°. The average amplitude of the signal, expressing the mean angular excursion throughout the movement cycles, is 59.1°. For the roll angle, the maximum value observed is 21.7°, whereas the minimum reached −20.3°. The peak points, corresponding to the plantarflexion phase, exhibited a mean value of 9.4°, while the

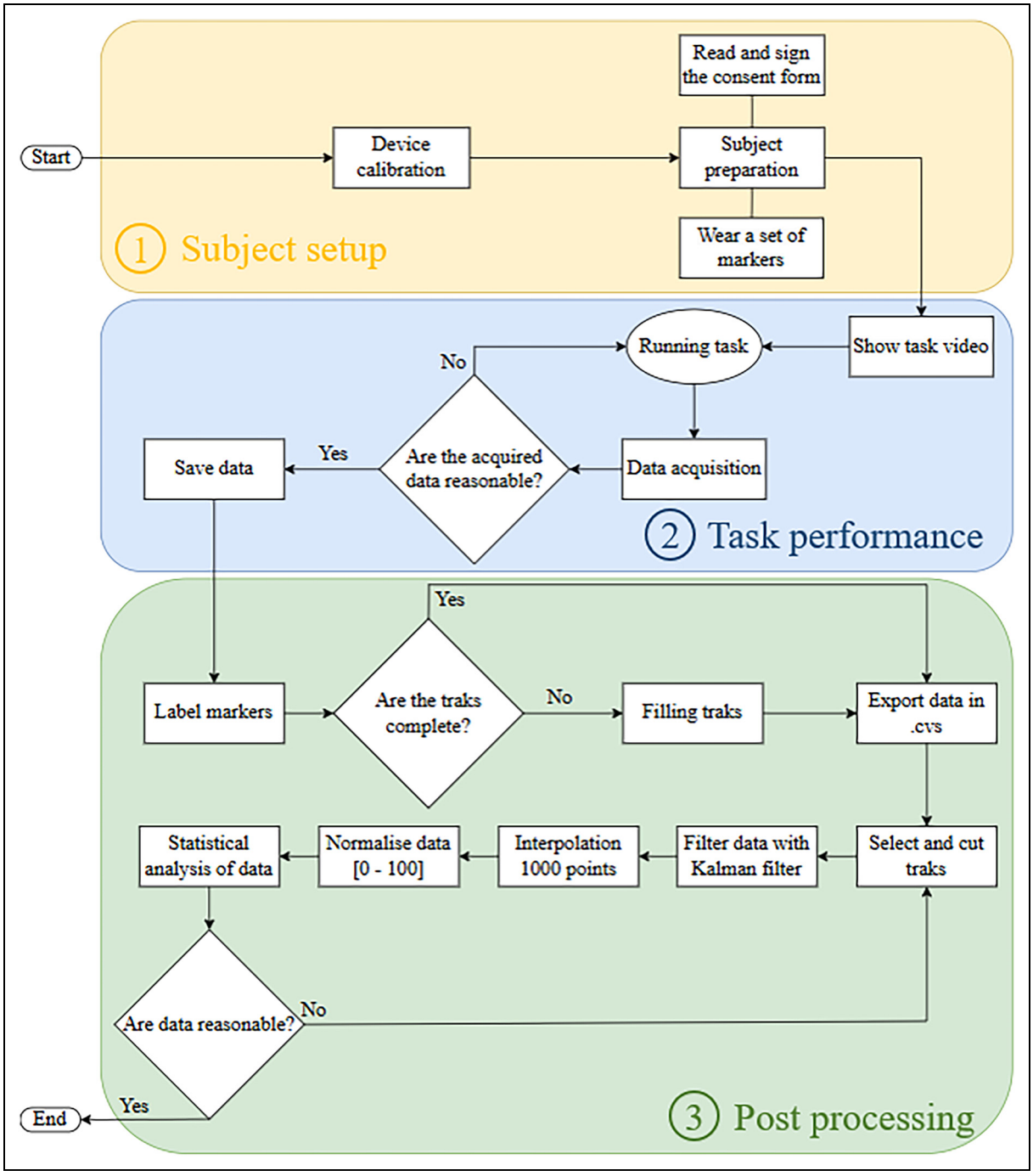

Figure 10. Flowchart of the proposed procedure.

valley points, related to the dorsiflexion phase, presented a mean value of −8.6°. The average amplitude of the signal, expressing the mean angular excursion throughout the movement cycles, is 18.0°. For the pitch angle, the maximum value observed is 17.8°, whereas the minimum reached −16.9°. The peak points, corresponding to the dorsiflexion phase, exhibited a mean value of 7.6°, while the valley points, related to the plantarflexion phase, presented a mean value of −6.1°. The average amplitude of the signal, expressing the mean angular excursion throughout the movement cycles, is 13.6°.

Table 3 reports the main significant value of pitch, roll and yaw during dorsiflexion/plantarflexion movements.

Dorsiflexion and plantarflexion showed the largest angular excursions, confirming the dominant role of sagittal-plane motion. Low intra-subject variability across repeated

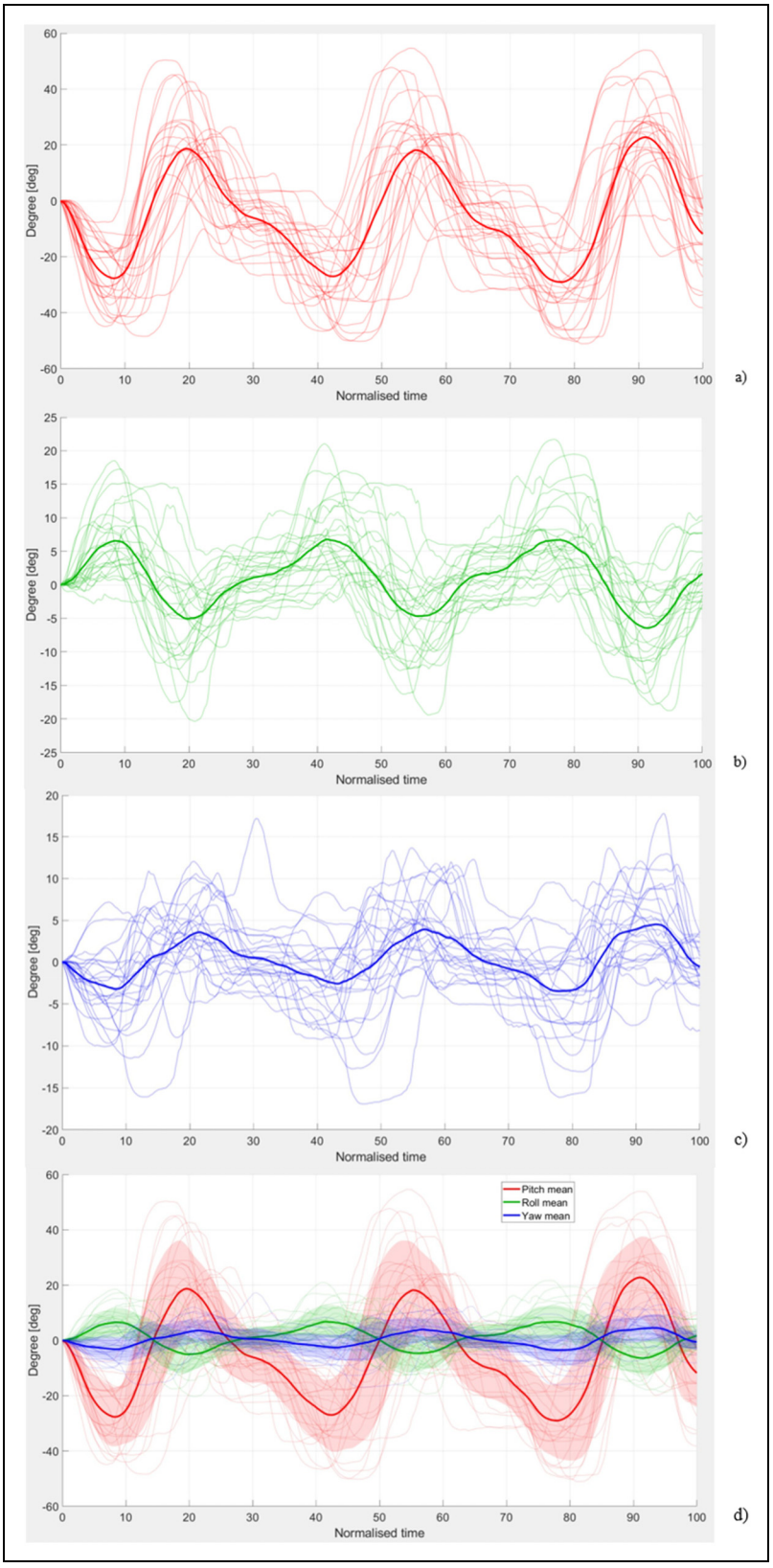

Figure 11. Dorsiflexion and plantarflexion movements of 34 subjects: (a) pitch angle and mean; (b) roll angle and mean; (c) yaw angle and mean; (d) pitch, roll and yaw angles together and mean ± one standard deviation.

Table 3. Main significant value of pitch, roll and yaw during dorsiflexion/plantarflexion movements.

	Pitch [deg]	Roll [deg]	Yaw [deg]
Max	54.6	21.7	17.8
Min	−51.9	−20.3	−16.9
Mean pick	26.7	9.4	7.6
Mean valley	−32.4	−8.6	−6.1
Range mean	59.1	18.0	13.6

trials demonstrates strong repeatability, while inter-subject differences reflect natural anatomical and neuromuscular variability. The presence of secondary roll and yaw components, despite the intended uniplanar task, highlights intrinsic joint coupling and supports the need for three-dimensional kinematic analysis.

The second movement analysed corresponds to inversion and eversion of the ankle (Figure 12). As with the previous case, this motion was examined by isolating the relevant data segments and processing them individually. Inversion–eversion movements are also characterised by a complex multi-axial behaviour, where the predominant rotation occurs around the mediolateral axis but is accompanied by secondary components along the other two axes. This coupling effect is evident in the plotted angular traces, which reveal minor but consistent cross-axis interactions.

The analysis therefore focused on the principal component associated with the inversion–eversion axis, in order to determine the effective ROM and evaluate the extent of inter-subject variability. For each test performed, the pitch, roll and yaw angles were considered separately, and the mean trace for each angle was computed across repetitions.

A summary chart reports the mean angular values (±one standard deviation) of the three components, together with the individual traces obtained from all 34 subjects.

Positive roll values correspond to eversion and negative values to inversion. For the secondary motions, positive pitch values were mainly associated with eversion and negative values with inversion; positive yaw values corresponded primarily to eversion and negative values to inversion. For the pitch angle, the maximum value observed is 46.5°, whereas the minimum reached −24.7°. The peak points, corresponding to the eversion phase, exhibited a mean value of 20.6°, while the valley points, related to the inversion phase, presented a mean value of −6.5°. The average amplitude of the signal, expressing the mean angular excursion throughout the movement cycles, is 27.0°. For the roll angle, the maximum value observed is 36.4°, whereas the minimum reached −54.0°. The peak points, corresponding to the eversion phase, exhibited a mean value of 18.0°, while the valley points, related to the inversion phase, presented a mean value of −19.4°. The average amplitude of the signal, expressing the mean angular excursion throughout the movement cycles, is 37.4°. For the pitch angle, the maximum value observed is 28.7°, whereas the minimum reached −31.8°. The peak points, corresponding to the eversion phase, exhibited a mean value of 16.5°, while the valley points, related to the inversion phase, presented a mean value of −18.2°. The average amplitude of the signal, expressing the mean angular excursion throughout the movement cycles, is 34.7°.

Table 4 reports the main significant value of pitch, roll and yaw during inversion/eversion movements.

Inversion and eversion exhibited strong coupling between roll and yaw components, making these movements difficult to isolate. Subjects consistently engaged multiple rotational axes even during single-plane tasks, as expected from subtalar joint geometry and muscular stabilisation. The consistency of these patterns across subjects confirms that the protocol captures physiological joint behaviour rather than measurement artefacts.

The final movement analysed corresponds to adduction and abduction of the ankle (Figure 13). As with the previous movements, the data were segmented according to the specific motion and analysed individually for each participant. Adduction–abduction involves primary rotation around the vertical axis, while minor rotations along the sagittal and frontal planes are also present, reflecting the intrinsic multi-axial nature of ankle kinematics. These secondary components are clearly observable in the angular traces provided.

The analysis concentrated on the principal component corresponding to the adduction–abduction axis in order to quantify the ROM for each subject. For each trial, the pitch, roll and yaw angles were extracted and analysed separately, and the mean trace for each angle was computed across repetitions.

A summary diagram presents the mean angular values (±one standard deviation) for all three components, along with the individual traces of the 34 participants.

Positive yaw values correspond to abduction and negative values to adduction. For the secondary motions, positive pitch values were mainly associated with abduction and negative values with adduction; positive roll values corresponded primarily to abduction and negative values to adduction. For the pitch angle, the maximum value observed is 26.9°, whereas the minimum reached −18.6°. The peak points, corresponding to the abduction phase, exhibited a mean value of 13.2°, while the valley points, related to the adduction phase, presented a mean value of −6.6°. The average amplitude of the signal, expressing the mean angular excursion throughout the movement cycles, is 19.7°. For the roll angle, the maximum value observed is 38.1°, whereas the minimum reached −39.3°. The peak points, corresponding to the abduction phase, exhibited a mean value of 19.3°, while the valley points, related to the adduction phase, presented a mean value of −21.8°. The average amplitude of the signal, expressing the mean angular excursion throughout

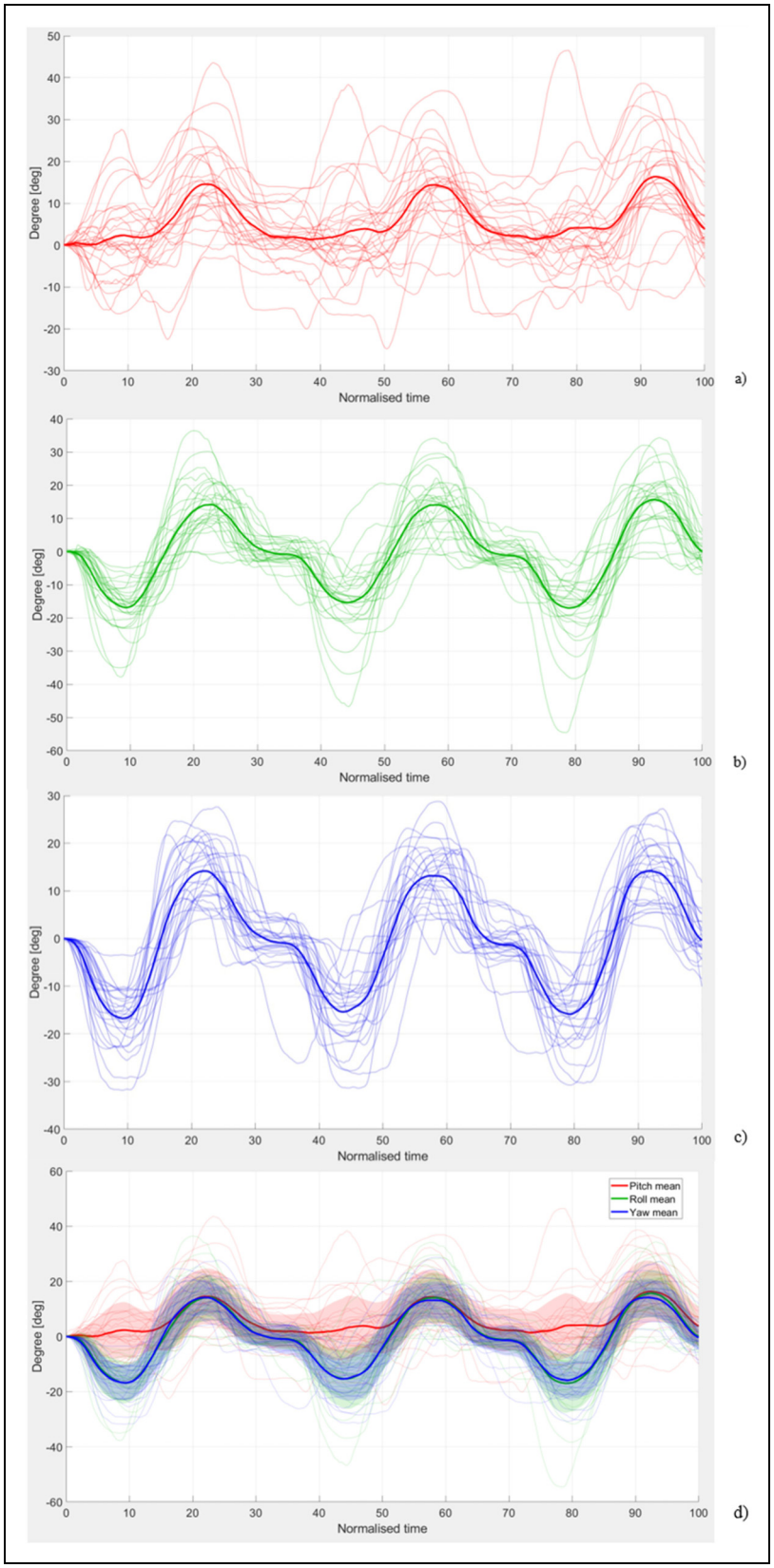

Figure 12. Inversion and eversion movements of 34 subjects: (a) pitch angle and mean; (b) roll angle and mean; (c) yaw angle and mean; (d) pitch, roll and yaw angles together and mean ± one standard deviation.

Table 4. Main significant value of pitch, roll and yaw during inversion/eversion movements.

	Pitch [deg]	Roll [deg]	Yaw [deg]
Max	46.5	36.4	28.7
Min	−24.7	−54.0	−31.8
Mean pick	20.6	18.0	16.5
Mean valley	−6.5	−19.4	−18.2
Range mean	27.0	37.4	34.7

the movement cycles, is 41.1°. For the pitch angle, the maximum value observed is 31.7°, whereas the minimum reached −24.7°. The peak points, corresponding to the abduction phase, exhibited a mean value of 13.1°, while the valley points, related to the adduction phase, presented a mean value of −15.2°. The average amplitude of the signal, expressing the mean angular excursion throughout the movement cycles, is 28.3°.

Table 5 reports the main significant value of pitch, roll and yaw during adduction/abduction movement.

Adduction and abduction further confirmed the multi-axis nature of ankle motion. Although yaw was dominant, consistent pitch and roll contributions were observed, indicating compensatory adjustments in the sagittal and frontal planes. These coupled rotations provide a more complete representation of ankle kinematics and support the use of the extracted trajectories in control-oriented applications.

An additional analysis focused on the relative movement between the participants' feet and the footwear (Figure 14). For all types of ankle movements, the absolute value of this slip was calculated, and the mean value across all repetitions was determined for each subject. The corresponding plots illustrate the individual traces of all 34 participants, along with the mean values and the observed ranges, including the maximum and minimum values recorded during the execution of each movement.

Furthermore, a comprehensive summary chart was generated to include all slip measurements across the three analysed movements. In this chart, the overall mean, as well as the maximum and minimum values recorded throughout the entire duration of the exercises, are reported. This analysis provides a quantitative assessment of the foot–shoe interface behaviour, highlighting inter-subject variability and the potential implications for movement accuracy and footwear design.

Although distance is, by definition, a positive quantity, in the previous figures the pattern of foot–shoe slip was represented after being shifted relative to the initial position, in order to provide a clearer visualisation of the relative displacement throughout the movement and to facilitate comparison across trials.

During the dorsiflexion and plantarflexion movement, the maximum relative displacement between the foot and the shoe reached 7.4 mm, while the minimum displacement was −4.7 mm. The mean displacement exhibited a maximum value of 0.6 mm and a minimum value of −0.4 mm.

During the inversion and eversion movement, the maximum relative displacement between the foot and the shoe reached 3.2 mm, while the minimum displacement was −4.7 mm. The mean displacement exhibited a maximum value of 0.4 mm and a minimum value of −0.7 mm.

During the adduction and abduction movement, the maximum relative displacement between the foot and the shoe reached 4.6 mm, while the minimum displacement was −4.0 mm. The mean displacement exhibited a maximum value of 0.3 mm and a minimum value of −0.8 mm.

During all the movements, the maximum relative displacement between the foot and the shoe reached 7.4 mm, while the minimum displacement was −4.7 mm. The mean displacement exhibited a maximum value of 0.2 mm and a minimum value of −0.5 mm.

Table 6 reports the main significant value of slip between foot and shoe during all the movements.

Clear separation between low intra-subject variability and higher inter-subject variability demonstrates that the protocol yields stable, repeatable measurements while preserving physiological diversity. This distinction is particularly relevant for rehabilitation and assistive systems that require robust yet user-adaptive reference trajectories.

These results collectively validate the robustness of the proposed protocol and provide the basis for interpreting functional ankle mobility in a reproducible three-dimensional framework.

Discussion

The present work provides an extensive characterisation of ankle kinematics through a standardised, reproducible protocol that combines high-resolution motion capture data with a clear anatomical and mechanical interpretation of joint behaviour. The findings confirm that the ankle joint exhibits inherently coupled motion patterns, where rotations along the primary axes are consistently accompanied by secondary angular displacements. This observation underscores the inadequacy of simplified planar analyses and highlights the importance of adopting three-dimensional, multi-axis approaches when quantifying human joint motion.

From a methodological standpoint, the adoption of a standardised marker configuration, uniform filtering and identical movement protocols across all participants ensures reproducibility and cross-laboratory comparability. This standardisation is one of the key outcomes of the work, addressing a significant gap in current ankle biomechanics research, where heterogeneous acquisition and processing methods often hinder meta-analysis and clinical translation.

The proposed methodology allowed a detailed examination of dorsiflexion/plantarflexion, inversion/eversion and adduction/abduction movements, revealing consistent intra-subject patterns and variable inter-subject responses. Such variability, which arises from natural anatomical

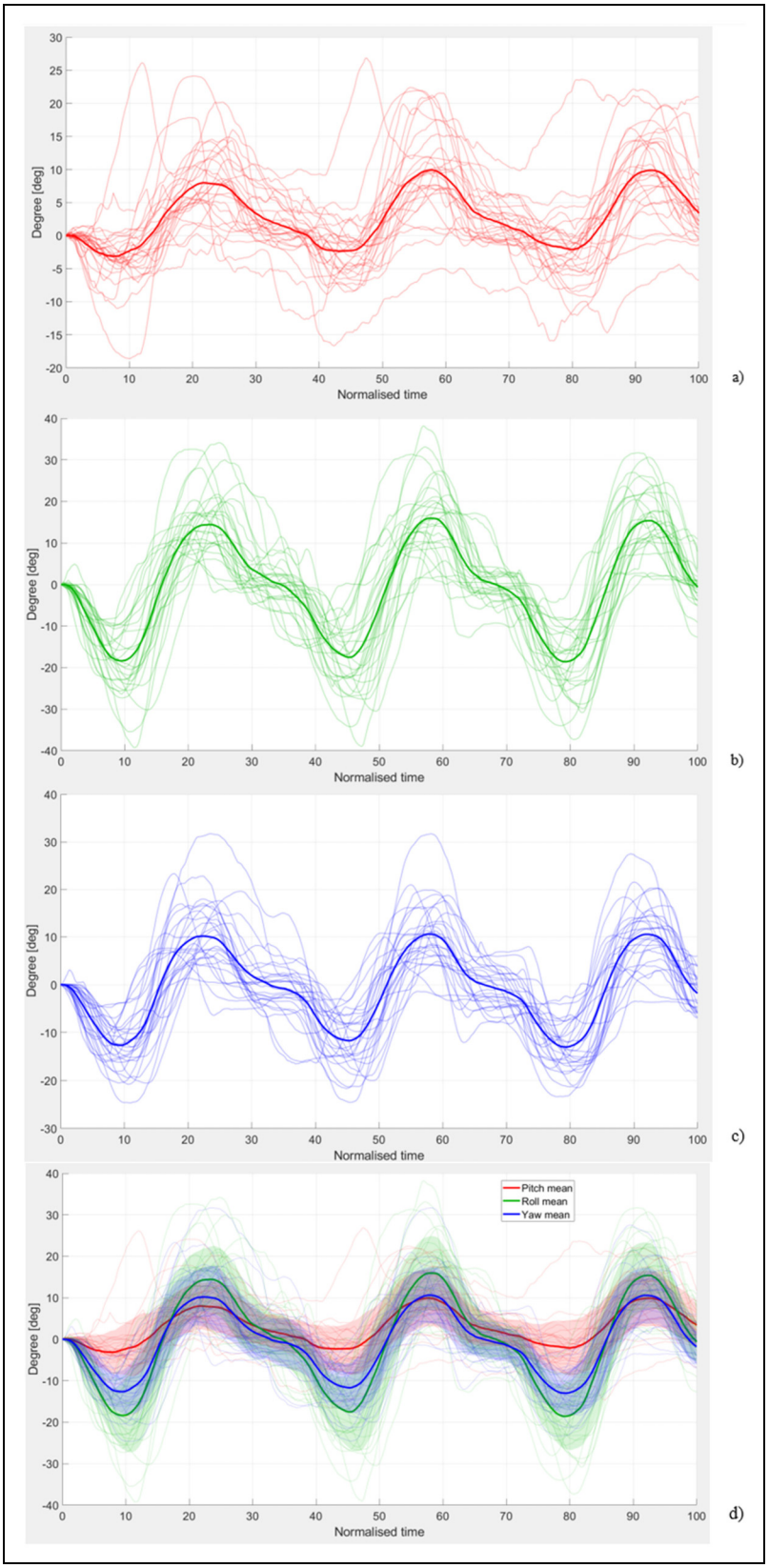

Figure 13. Adduction and abduction movements of 34 subjects: (a) pitch angle and mean; (b) roll angle and mean; (c) yaw angle and mean; (d) pitch, roll and yaw angles together and mean ± one standard deviation.

Table 5. Main significant value of pitch, roll and yaw during adduction/abduction movements.

	Pitch [deg]	Roll [deg]	Yaw [deg]
Max	26.9	38.1	31.7
Min	−18.6	−39.3	−24.7
Mean pick	13.2	19.3	13.1
Mean valley	−6.6	−21.8	−15.2
Range mean	19.7	41.1	28.3

differences, including joint laxity, tendon stiffness and muscle coordination, represents a realistic depiction of the population's biomechanical diversity. Establishing this normative variability is fundamental for future comparative studies involving pathological conditions such as chronic ankle instability, arthritis or post-surgical rehabilitation.

As shown in Figure 11, dorsiflexion and plantarflexion represent the most prominent movements of the ankle. Indeed, the ROM along the pitch axis is significantly larger than that of roll and yaw during these movements. This indicates that the primary movement occurs predominantly in the sagittal plane. However, secondary rotations along the roll and yaw axes are also present, though with much smaller amplitudes, suggesting subtle coupled motions in other planes. This reflects the natural multi-axial behaviour of the ankle joint, even during what is largely a uniplanar movement. The pitch angle exhibits maximum and minimum values of approximately 54.6° (dorsiflexion) and −51.9° (plantarflexion), respectively, although the values reported in the literature[41–43] typically indicate approximately 40°–50° for plantarflexion and 20°–30° for dorsiflexion, this discrepancy can be justified by considering that, during task execution, participants did not all begin from an identical starting position, nor did they necessarily return to the same initial position upon completion. Such variations in initial and final joint positioning may have influenced the recorded ROM, accounting for the observed differences from reference values. The mean peak and mean valley values for pitch, 26.7° and −32.4° suggest a slight asymmetry, with greater plantarflexion than dorsiflexion, which reflects the natural predominance of plantarflexion, in agreement with data reported in the literature.[41–43] Range mean value represents the average ROM and is, as expected, greater in pitch, 59.1°.

Inversion and eversion appear to be the most challenging single-axis movements to perform in isolation. Figure 12 clearly shows that all three angular components, pitch, roll and yaw, are involved. Notably, roll and yaw exhibit very similar patterns and almost overlap, indicating coupled rotations in the frontal and transverse planes. The pitch angle shows positive values near the end of both movements. This can be explained biomechanically: while attempting to rotate the foot along axes parallel to the floor, the toes are slightly lifted, producing an observable change in the sagittal plane. This highlights the difficulty of achieving a "pure" inversion or eversion without secondary motions. Although the maximum 36.4° (inversion) and minimum −54.0° (eversion) values are considerably higher than those reported in the literature,[41–43] it should be noted that not all participants started and finished the task at the same point. Given that the movement was performed freely, the mean peak 18.0° and the mean valley −19.4° values fall within a range of approximately 35°, data reported in literature[41–43] and the average ROM, 37.4°, which is very similar to that of yaw, since, as previously noted, it is difficult to perform inversion and eversion movements without simultaneously inducing a similar rotation around the vertical axis.

Similarly, during adduction and abduction, roll and yaw display very similar trends, suggesting that these movements also involve coupled rotations in multiple planes (Figure 13). The pitch angle assumes positive values at the end of abduction (movement outward) and negative values at the end of adduction (movement inward). This pattern indicates that even in what is intended as a primarily transverse-plane movement, there is a consistent sagittal-plane contribution, likely due to the anatomy of the ankle and the need to stabilise the foot during the motion. The yaw angle exhibits maximum and minimum values of approximately 31.7° (adduction) and −24.7° (abduction), respectively, mean pick 13.1° and mean valley −15.2° and range mean 28.3° that are aligner to the range of approximately 30° reported in literature.[41–43]

Overall, these data demonstrate that ankle movements are rarely truly isolated to a single axis. Even in movements that are conceptually uniplanar, small but measurable secondary rotations occur along the other axes. These secondary rotations may reflect the complex geometry of the ankle joint, neuromuscular control strategies or biomechanical constraints of the foot and leg. Understanding these coupled motions is important for biomechanical modelling, clinical assessment and rehabilitation planning.

Another particularly relevant contribution of this work is the quantitative assessment of the relative displacement between the foot and the shoe (Figure 14). While most kinematic studies assume rigid coupling between these elements, our results demonstrate measurable slip values that vary across movement types. This decoupling can significantly affect the interpretation of joint kinematics, especially in experimental setups where markers are mounted on the shoe rather than directly on the skin. Understanding this relative motion is essential not only for improving data accuracy but also for optimising footwear design, orthotic devices and exoskeleton interfaces. The slip behaviour may also serve as an indicator of dynamic stability, grip efficiency and subject comfort during functional movements. From the presented data, it can be observed that the maximum and minimum relative displacement between the foot and the shoe occurs during

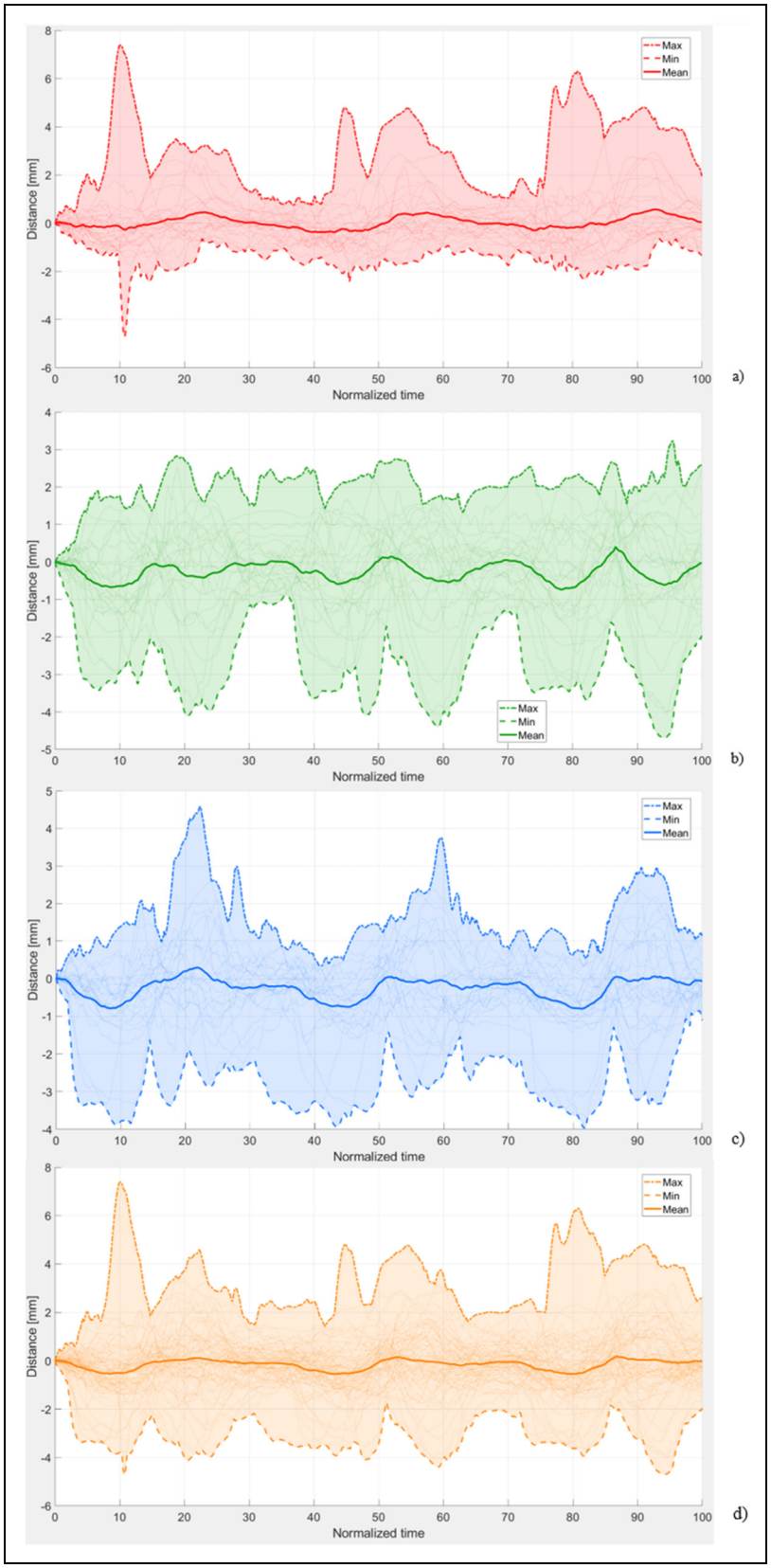

Figure 14. Magnitude of the slip between the foot and the shoe of 34 subjects: (a) dorsiflexion/plantarflexion movements; (b) inversion/eversion movements; (c) adduction/abduction movements; (d) sum of all the three movements.

Table 6. Main significant value of slip between foot and shoe during all the movements.

	Dorsiflexion/ plantarflexion slip [mm]	Inversion/ eversion slip [mm]	Adduction/ abduction slip [mm]	All movements slip [mm]
Max	7.4	3.2	4.6	7.4
Min	−4.7	−4.7	−4.0	−4.7
Mean max	0.6	0.4	0.3	0.2
Mean min	−0.4	−0.7	−0.8	−0.5

dorsiflexion and plantarflexion, 7.4 mm and −4.7 mm respectively, which, as previously discussed, represent the most prominent movements of the ankle. Despite being the largest ankle motion, the displacement remains relatively small, on the order of millimetres. This indicates that the shoe used maintained a sufficiently snug fit on the subject's foot, minimising slippage during movement. From the graphical tracking of the maximum and minimum values, a certain regularity can be observed in the repetition of the three movements for each task, indicating that the maximum displacement occurs precisely at the point of movement reversal.

These observations are important for interpreting the kinematic data, as they confirm that the measured ankle rotations primarily reflect the motion of the foot itself rather than relative motion between the foot and the footwear. Maintaining minimal foot–shoe displacement is crucial in biomechanical experiments to ensure accurate capture of true joint kinematics. Furthermore, the small magnitude of slippage observed suggests that the footwear provided consistent mechanical coupling to the foot, which is essential for reliable motion analysis and for reducing potential artefacts in the recorded angular data.

The experimental setup, based on independent local reference frames (shank, foot and shoe), minimised soft-tissue artefacts and allowed an accurate representation of intersegmental motion. The use of the UR kinematic model, representing the tibiotalar and subtalar joints, proved effective in describing the complex rotational coupling mechanisms that govern ankle movement. Furthermore, the approach supports a modular interpretation of the ankle as a multi-joint system, which is beneficial for both biomechanical analysis and the design of mechatronic rehabilitation systems.

From a clinical perspective, the proposed standardised framework provides a valuable tool for the quantitative assessment of ankle joint function. By capturing precise three-dimensional kinematic data, it enables clinicians to identify functional impairments, asymmetries or compensatory movement patterns that may not be evident through visual observation alone. The ability to compute individualised ROM, variability and coupling effects across movement planes offers a robust basis for monitoring rehabilitation progress and tailoring interventions to each patient's biomechanical profile. This approach supports the development of evidence-based, patient-specific rehabilitation strategies and could serve as a reference for establishing normative datasets in both healthy and pathological populations.

From a control perspective, the standardised three-dimensional ankle kinematic data generated by the proposed protocol are directly applicable to modern position tracking control schemes used in rehabilitation robotics.

Compared with existing ankle kinematics studies, the present work introduces several novel elements. Traditional biomechanical investigations primarily report ROM values along individual anatomical planes or focus on gait-related movements, often using heterogeneous marker configurations and processing pipelines. While these approaches provide valuable descriptive data, they limit reproducibility and cross-study comparison. In contrast, the proposed protocol establishes a standardised marker configuration and local reference frame definition that enable consistent three-dimensional kinematic reconstruction across subjects and laboratories.

Although a formal closed-loop stability analysis is beyond the scope of this experimental study, stability-related properties can be assessed from a kinematic perspective. The extracted ankle trajectories are smooth, bounded and highly repeatable, with low intra-subject variability and physiologically bounded inter-subject differences, supporting their suitability as stable reference inputs for robust trajectory and position tracking control frameworks.

The present work is limited to kinematic analysis and does not include dynamic modelling or estimation of joint torques. Torque computation requires subject-specific inertial properties, muscle-tendon dynamics and external loads, which are beyond the scope of the proposed protocol. Nevertheless, the standardised three-dimensional kinematic trajectories obtained here provide suitable reference inputs for future inverse dynamics analyses and torque- or impedance-controlled rehabilitation systems.

This work focuses on isolated ankle movements under controlled conditions and therefore does not address long-term effects of repetitive motion or fatigue. Comprehensive gait analysis and collision avoidance are also beyond the scope of this work, as they require dynamic, task-dependent models involving whole-body coordination, ground interaction and environmental sensing. Future work will extend the proposed kinematic framework to gait and dynamic scenarios to investigate long-term motion behaviour and collision-aware control strategies.

In this work, uncertainties arise mainly from measurement noise, marker placement variability in different subjects and subject-specific anatomy, whose effects are addressed through experimental design, signal processing and repeatability analysis rather than explicit control

compensation. The low intra-subject variability and consistent secondary rotational patterns across trials indicate that these disturbances have a limited and bounded effect on the extracted kinematics, while inter-subject variability reflects true physiological differences. These results demonstrate that the proposed protocol produces smooth, repeatable trajectories that are inherently robust to experimental uncertainties and suitable for control-oriented applications.

In the context of intelligent rehabilitation robotics, the standardised motion capture data generated through this protocol can serve as a foundation for data-driven modelling and control. The availability of consistent, high-quality kinematic datasets allows for the training of artificial intelligence algorithms capable of recognising movement patterns, detecting abnormalities and adapting therapeutic assistance in real time. Integrating this framework into robotic platforms or wearable devices could facilitate adaptive control strategies that respond dynamically to the user's motion, improving safety, comfort and efficacy during rehabilitation exercises. Ultimately, the combination of standardised experimental biomechanics and AI-based analysis paves the way for next-generation personalised rehabilitation systems.

Conclusion

This work introduced and validated a comprehensive, standardised protocol for the three-dimensional evaluation of ankle kinematics using a high-resolution motion capture system. The experimental campaign conducted on 34 healthy participants demonstrated the reliability of the proposed methodology in capturing the full range of ankle motion across sagittal, frontal and transverse planes confirming the robustness of the proposed measurement and data processing framework. The ankle joint exhibited the greatest mobility in the frontal plane, with a maximum pitch angle of 106.5°, while maximum roll and yaw angles reached 90.4° and 60.5°, respectively. Dorsiflexion and plantarflexion were dominated by pitch motion, with an average range of 59.1° in pitch compared to 18.0° in roll and 13.6° in yaw. Inversion and eversion showed a more evenly distributed motion pattern, with average angular displacements ranging between 27.0° and 37.4° across pitch, roll and yaw axes. Abduction and adduction were primarily characterised by roll motion, averaging 41.1° in roll, 28.3° in yaw and 19.7° in pitch. The results, moreover, confirmed that even during isolated movements, the ankle exhibits complex multi-planar behaviour, emphasising the interdependence of its anatomical structures. The smooth and continuous ankle trajectories extracted from the proposed protocol illustrate that the generated kinematic profiles are well suited for robust trajectory and position tracking strategies. The time-normalised and noise-filtered angular trajectories provide reliable reference signals that can be directly employed in advanced control frameworks, where accurate and repeatable joint motion profiles are essential to ensure stability, tracking precision and user safety. The stability-related properties of the generated trajectories, including smoothness, boundedness and repeatability, further support their suitability for stable and robust trajectory tracking applications in rehabilitation and assistive robotic systems.

The protocol's strength lies in its capacity to isolate and analyse primary and secondary motion components while maintaining consistency through precise marker placement and local reference frame construction. The observed consistency of the primary motion components, together with the quantification of secondary coupled rotations, supports the use of these trajectories in control schemes designed to handle multi-axis motion and anatomical variability. The inclusion of the foot–shoe slip analysis represents an innovative element that broadens the biomechanical understanding of the ankle–foot interface and provides valuable insights for footwear design and exoskeleton alignment.

Beyond its immediate biomechanical relevance, the work establishes a methodological benchmark that can facilitate standardised data acquisition across laboratories and research centres. Such reproducibility is critical for developing shared databases, validating computational models and ensuring consistent metrics for clinical diagnosis and rehabilitation monitoring. By providing standardised, high-quality three-dimensional motion data, this framework bridges experimental biomechanics and modern control-oriented rehabilitation technologies.

Future work will extend this protocol to pathological populations and dynamic conditions, integrating kinetic and electromyographic data to characterise the neuromechanical control of the ankle. Investigation of correlations between ankle joint movements or foot–shoe slip and participant characteristics (age, gender, height, body mass) will also be addressed in a separate, dedicated study. The combination of standardised experimental data and advanced computational tools, including AI-driven pattern recognition, holds promise for creating predictive models capable of supporting personalised rehabilitation and adaptive assistance in wearable robotic systems.

In conclusion, the proposed framework represents a significant step toward the harmonisation of ankle motion analysis methods, bridging the gap between experimental biomechanics, clinical practice and the design of intelligent assistive devices.

Ethics approval and consent to participate

The protocol has been approved by the Ethics Committee of Swansea University with Research Ethics Approval Number: 1 2024 11492 10405. Informed consent was obtained from all subjects involved in the study.

ORCID iDs

Giovanni Mastrangelo https://orcid.org/0009-0002-0787-3448
Betsy Dayana Marcela Chaparro Rico https://orcid.org/0000-0002-6874-2508
Chelsea Starbuck https://orcid.org/0000-0001-6266-2876
Matteo Russo https://orcid.org/0000-0002-8825-8983
Marco Ceccarelli https://orcid.org/0000-0001-9388-4391
Daniele Cafolla https://orcid.org/0000-0002-5602-1519

Author contributions

G.M. led and performed all aspects of the research, including conceptualisation, data curation, formal analysis, funding acquisition, investigation, methodology, project administration, resources, supervision, validation, visualisation, and writing both the original draft and final manuscript. D.C. contributed to conceptualisation, formal analysis, visualisation, funding acquisition, investigation, methodology, project administration, resources, supervision, as well as writing the original and final versions of the manuscript. C.S. contributed resources and validation. M.R. and M.C. provided supervision, contributed to methodology and project administration, and participated in formal analysis. B.D.M.C.-R. contributed in conceptualisation, investigation, methodology and visualisation. All authors collaborated to ensure the study's accuracy and quality, and to prepare the final manuscript.

Funding

The authors received no financial support for the research, authorship, and/or publication of this article.

Declaration of conflicting interests

The authors declared no potential conflicts of interest with respect to the research, authorship, and/or publication of this article.

Availability of data and materials

The raw data supporting the conclusions of this article will be made available by the authors, without undue reservation on request.

References

1. Hall S. *Basic Biomechanics*. New York, NY, USA: McGraw-Hill Higher Education, 2014.
2. Muro-de-la-Herran A, Garcia-Zapirain B and Mendez-Zorrilla A. Gait analysis methods: an overview of wearable and non-wearable systems, highlighting clinical applications. *Sensors* 2014; 14: 3362–3394.
3. Hussain S, Jamwal PK, Vliet PV, et al. Robot assisted ankle neuro-rehabilitation: state of the art and future challenges. *Expert Rev Neurother* 2021; 21: 111–121.
4. Xu M, Hua Y, Li Y, et al. Development of an ankle assistive robot with instantly gait-adaptive method. *J Robot Mechatron* 2023; 35: 669–683.
5. Zhetenbayev N, Ceccarelli M and Russo M. Design and testing of almaty ankle exoskeleton v.2. *Int J Mech Control* 2025; 26: 129–144.
6. Xia H, Kwon J, Pathak P, et al. Design of A multi-functional soft ankle exoskeleton for foot-drop prevention, propulsion assistance, and inversion/eversion stabilization. *2020 8th IEEE RAS/EMBS International Conference for Biomedical Robotics and Biomechatronics (BioRob)*, New York, NY, USA, 2020, pp. 118–123, https://doi.org/10.1109/BioRob49111.2020.9224420
7. Shi K, Wang Z, Yan C, et al. Design and performance analysis of the 4UPS-RRR parallel ankle rehabilitation mechanism. *Mech Sci* 2024; 15: 417–430. https://doi.org/10.5194/ms-15-417-2024
8. Chen ET, McInnis KC and Borg-Stein J. Ankle sprains: evaluation, rehabilitation, and prevention. *Curr Sports Med Rep* 2019; 18: 217–223.
9. Leardini A, O'Connor JJ and Giannini S. Biomechanics of the natural, arthritic, and replaced human ankle joint. *J Foot Ankle Res* 2014; 7: 16. https://doi.org/10.1186/1757-1146-7-8
10. Rodríguez-León JF, Chaparro-Rico BDM, Russo M, et al. An autotuning cable-driven device for home rehabilitation, *J Healthc Eng*, 2021, 6680762, 15 pages, 2021. https://doi.org/10.1155/2021/6680762
11. Hussain S, Jamwal PK, Vliet PV, et al. Robot assisted ankle neuro-rehabilitation: state of the art and future challenges. *Expert Rev Neurother* 2021; 21: 111–121.
12. Wagemans J, Bleakley C, Taeymans J, et al. Exercise-based rehabilitation reduces reinjury following acute lateral ankle sprain: a systematic review update with meta-analysis. *PLoS ONE* 2022; 17: e0262023.
13. Ceccarelli M. Challenges in service robot devices for elderly motion assistance. *Robotica* 2024; 42: 1–14. https://doi.org/10.1017/S0263574724001528
14. Russo M and Ceccarelli M. Analysis of a wearable robotic system for ankle rehabilitation. *Machines* 2020; 8: 48.
15. Shi K, Wang Z, Yan C, et al. Design and performance analysis of the 4UPS-RRR parallel ankle rehabilitation mechanism. *Mech Sci* 2024; 15: 417–430.
16. Xu M, Hua Y, Li Y, et al. Development of an ankle assistive robot with instantly gait-adaptive method. *J Robot Mechatron* 2023; 35: 669–683.
17. Xia H, Kwon J, Pathak P, et al. Design of a multi-functional soft ankle exoskeleton for foot-drop prevention, propulsion assistance, and inversion/eversion stabilization. In *Proc. 8th IEEE RAS/EMBS Int. Conf. Biomed. Robot. Biomechatronics (BioRob)*, New York, NY, USA, 2020, pp. 118–123. https://doi.org/10.1109/BioRob49111.2020.9224420
18. Wade L, Needham L, McGuigan P, et al. Applications and limitations of current markerless motion capture methods for clinical gait biomechanics. *PeerJ* 2022; 10: e12995.
19. Lam WWT, Tang YM and Fong KNK. A systematic review of the applications of markerless motion capture (MMC) technology for clinical measurement in rehabilitation. *J NeuroEngineering Rehabil* 2023; 20: 57.
20. Ma P, Bian Q, Kim JM, et al. Measuring lower-limb kinematics in walking: wearable sensors achieve comparable reliability to motion capture systems and smartphone cameras. *Sensors* 2025; 25: 2899.

21. Mastrangelo G, Rico BDMC, Russo M, et al. An Experimental Characterization of Human Ankle Motion. In: Laribi MA, Carbone G, Pisla D and Zeghloul S (eds) *New Trends in Medical and Service Robotics. MESROB 2025. Mechanisms and Machine Science*, vol 186. Springer, Cham, 2025, pp. 170–180. https://doi.org/10.1007/978-3-031-96081-9_18
22. Mastrangelo G, Rico BDMC, Starbuck C, et al. A Protocol for Analysing Ankle Motion Data: A Standardized Approach to Kinematic Assessment. In: Cafolla D, Rittman T and Ni H (eds) *Artificial Intelligence in Healthcare. AIiH 2025. Lecture Notes in Computer Science*, vol 16039. Springer, Cham, 2026, pp. 232–243. https://doi.org/10.1007/978-3-032-00656-1_17
23. Zhang M, Davies TC and Xie S. Effectiveness of robot-assisted therapy on ankle rehabilitation–a systematic review. *J Neuroeng Rehabil* 2013; 10: 30.
24. Russo M, Chaparro-Rico B, Pavone L, et al. A bioinspired humanoid foot mechanism. *Appl Sci* 2021; 11: 1686.
25. Alawad NA, Humaidi AJ and Alaraji AS. Sliding mode-based active disturbance rejection control of assistive exoskeleton device for rehabilitation of disabled lower limbs. *An Acad Bras Cienc* 2023; 95: e20220680.. PMID: 37341275.
26. Brockett CL and Chapman GJ. Biomechanics of the ankle. *Orthop Trauma* 2016; 30: 232–238.
27. Leardini A, O'Connor JJ and Giannini S. Biomechanics of the natural, arthritic, and replaced human ankle joint. *J Foot Ankle Res* 2014; 7: 8.
28. Hemmerich A, Brown H, Smith S, et al. Hip, knee, and ankle kinematics of high range of motion activities of daily living. *J Orthopaed Res : Off Publ Orthopaedic Res Soc* 2006; 24: 770–781.
29. Hussain S, Jamwal PK, Vliet PV, et al. Robot assisted ankle neuro-rehabilitation: state of the art and future challenges. *Expert Rev Neurother* 2021; 21: 111–121.
30. Zhang J, Yang S, Liu C, et al. Configuration and kinematics of a 3-DOF generalized spherical parallel mechanism for ankle rehabilitation. *Chin J Mech Eng* 2024; 37: 24.
31. Procter P and Paul JP. Ankle joint biomechanics. *J Biomech* 1982; 15: 627–634.
32. *Kinesiology – The Skeletal System and Muscle Function*, 3rd ed. Amsterdam, The Netherlands: Elsevier, 2017.
33. Dawe EJC and Davis J. Anatomy and biomechanics of the foot and ankle. *Orthop Trauma* 2011; 25: 279–286.
34. Brockett CL and Chapman GJ. Biomechanics of the ankle. *Orthop Trauma* 2016; 30: 232–238.
35. Vicon Motion Capture system, https://www.vicon.com/, Visited on October 2025.
36. Nexus. https://www.vicon.com/software/nexus/, Visited on October 2025.
37. Davis RB III, Ounpuu S, Tyburski D, et al. A gait data collection and reduction technique. *Hum Mov Sci* 1991, 10: 575–587,
38. Zhang J, Yang S, Liu C, et al. Configuration and kinematics of a 3-DOF generalized spherical parallel mechanism for ankle rehabilitation. *Chin J Mech Eng* 2024; 37: 24.
39. MATLAB R2024b by The MathWorks, Inc. https://www.mathworks.com/products/matlab.html, Visited on October 2025.
40. Ceccarelli M. *Fundamentals of Mechanics of Robotic Manipulation*. London, UK: Springer, 2022.
41. Siegler S, Chen J and Schneck CD. The three-dimensional kinematics and flexibility characteristics of the human ankle and subtalar joints-part I: kinematics. *J Biomech Eng* 1988; 110: 364–373.
42. Roaas A and Andersson GB. Normal range of motion of the hip, knee and ankle joints in male subjects, 30–40 years of age. *Acta Orthop Scand* 1982; 53: 205–208.
43. Hemmerich A, Brown H, Smith S, et al. Hip, knee, and ankle kinematics of high range of motion activities of daily living. *J Orthop Res* 2006; 24: 770–781.